Available online at www.sciencedirect.com

jmr&t
Journal of Materials Research and Technology

journal homepage: www.elsevier.com/locate/jmrt

Original Article

Ti-containing hybrid mesoporous organosilicas as photocatalysts for H_2 production from ethanol

Yan Wang [a], Narcís Homs [a,b], Pilar Ramírez de la Piscina [a,*]

[a] Departament de Química Inorgànica i Orgànica, Secció de Química Inorgànica & Institut de Nanociència i Nanotecnologia (IN2UB), Universitat de Barcelona, Martí i Franquès 1, 08028 Barcelona, Spain
[b] Catalonia Institute for Energy Research (IREC), Jardins de les Dones de Negre 1, 08930 Barcelona, Spain

ARTICLE INFO

Article history:
Received 10 June 2021
Accepted 22 July 2021
Available online 27 July 2021

Keywords:
Renewable H_2
Ti-PMO photocatalysts
Microwave synthesis
H_2 photo-production
Ethanol photo-transformation
Periodic mesoporous organosilicas

ABSTRACT

A series of complex organic-inorganic mesoporous materials were successfully synthesized by a microwave-assisted method that allowed the preparation of periodic mesoporous organosilicas (PMOs) with Ti (IV) forming part of the structure (Ti-PMOs). Materials were characterized using N_2 adsorption–desorption isotherms, powder X-ray diffraction (XRD), transmission and high resolution transmission electron microscopy (TEM and HRTEM), Raman, infrared, UV–visible diffuse reflectance (UV–vis RDS), X-ray photoelectron (XPS), photoluminescence (PL) and electrochemical impedance (EIS) spectroscopy, and transient photocurrent measurements. Samples labeled Ti10-PMO, Ti20-PMO and Ti40-PMO (with Si/Ti molar ratio of about 10, 20 and 40), showed crystal-like characteristics and high specific surface area (742–829 m^2g^{-1}). Ti-PMOs were studied in the photocatalytic H_2 evolution from an aqueous ethanol solution under UV–visible irradiation. Ti-PMOs showed a better photocatalytic behavior than PMO and this is related with the presence of tetrahedral Ti(IV) in the PMOs network. Ti-PMOs displayed a lower barrier for the electron transfer and a more efficient charge separation than PMO. The highest H_2 production was obtained with Ti20-PMO photocatalyst; after 4 h of irradiation, 2042 μmol H_2 g_{cat}^{-1} were obtained, which was about 20 times higher than that obtained with a reference commercial TiO_2 (P25).

1. Introduction

Nowadays there is a severe concern regarding climate change and the use of fossil fuels in the energy scenario. This has attracted considerable interest in both the use of renewable sources, including biomass, and the development of new energy vectors, such as H_2. In this context, the photocatalytic production of hydrogen from biomass-derived alcohols is considered a highly desirable source for renewable hydrogen production [1–5]. Research for efficient photocatalytic systems is a hot topic under continuous progress; diverse semiconductor materials, mainly those based on TiO_2 [6,7], have been widely studied as photocatalysts for hydrogen production.

The high surface area, uniform porous array and long-range structure of ordered mesoporous materials make

* Corresponding author.
E-mail address: pilar.piscina@qi.ub.edu (P. Ramírez de la Piscina).
https://doi.org/10.1016/j.jmrt.2021.07.104

them interesting candidates to be used as photocatalysts [8]. The incorporation of titanium in the framework of mesoporous zeolites such as MCM-41 has revealed these materials as promising catalysts for different photocatalytic processes [9,10]. Hybrid materials such as metal organic frameworks (MOFs) have been also envisaged as versatile materials for designing heterogeneous photocatalysts [11]. In these systems, the capability of transferring the photogenerated electrons avoiding the electron–hole recombination is of main importance; a strong ligand–metal charge transfer (LMCT) could avoid the recombination of photoinduced electron–hole pairs, favoring the photocatalytic action of the material [12]. Titanium-containing MOFs (Ti-MOFs) and TiO_2/MOF composites have been considered appropriate photocatalysts for different processes [13,14]. A synergic effect between different conjugated porous polymers (CPPs) and TiO_2 in CPP-TiO_2 hybrid systems has been demonstrated useful for hydrogen evolution using methanol as sacrificial agent [12,15].

Periodically ordered mesoporous organosilicas (PMOs) are also hybrid materials [16–19], in which titanium could be introduced and be used as photocatalysts [20]. PMOs are hybrid organic-inorganic porous materials with $O_{1,5}$-Si-R-Si-$O_{1,5}$ units covalently bonded forming the pore walls. Considering that the presence of π-conjugated bridging groups could make these materials appropriate for light absorption, harvesting, and photo-induced electron and hole transportation [21–23] and that the presence of Ti(IV) centers could improve their photocatalytic properties, in this work we report the synthesis and characterization of new Ti-containing biphenylene-bridged PMOs materials (Ti-PMOs) with Ti wt%<2.

The Ti-PMOs reported in this work have crystal-like wall structure and high surface area, they are studied in the photocatalytic transformation of aqueous ethanol solutions without the assistance of noble metal co-catalyst. The use of sacrificial ethanol allows the use of a biomass-derived substrate and could have several advantages in terms of sustainability. In particular, bioethanol is highly attractive because its production is well established due to its current use as biofuel in internal combustion engines. Besides H_2 production, the sacrificial (ethanol) oxidation process could rend other valorized compounds, such as acetone or 2,3 butanediol, as we have recently reported using other TiO_2-based photocatalysts [24–26]. The effectiveness in the photocatalytic H_2 production of the new Ti-PMOs studied in this work, which depended on the Ti content, is related with the lower barrier for the electron transfer and the higher charge separation efficiency produced by the presence of Ti(IV) in the PMOs framework.

2. Materials and methods

2.1. Synthesis and characterization of photocatalysts

Biphenylene-bridged Ti-PMOs, with Si/Ti molar ratios of about 10, 20 and 40 (Ti10-PMO, Ti20-PMO and Ti40-PMO) were prepared on the basis of the method proposed for the biphenylene-bridged silsesquioxane silica with crystal-like pore walls, using 4,4′bis(triethoxysilyl)biphenyl and octadecyltrimethylammonium chloride as surfactant in basic media [27]. In the present work, Ti was introduced by addition to the initial synthesis mixture of the appropriate amount of tetrabutyl titanate in 2-propanol solution, and the suspension was heated at 100 °C with microwaves. After filtration, the surfactant was removed and the product dried at 100 °C. For comparative purposes, a non-containing Ti sample (PMO) was also prepared. Scheme 1 depicts the synthetic procedure, additional details are given in the Supplementary Material (Experimental methods).

The composition of photocatalysts was determined from chemical analysis and the materials were characterized by different techniques: N_2 adsorption isotherms (S_{BET}), powder X-ray diffraction (XRD), transmission and high resolution electron microscopy (TEM-HRTEM), Raman and infrared spectroscopy, and UV–vis diffuse reflectance (UV–vis DRS), X-ray photoelectron (XPS) spectroscopy. The photoelectrochemical properties were determined by photoluminescence (PL) and electrochemical impedance (EIS) spectroscopy and transient photocurrent measurements. Complete details for the instruments used for the characterization are given in the Supplementary Material (Experimental methods).

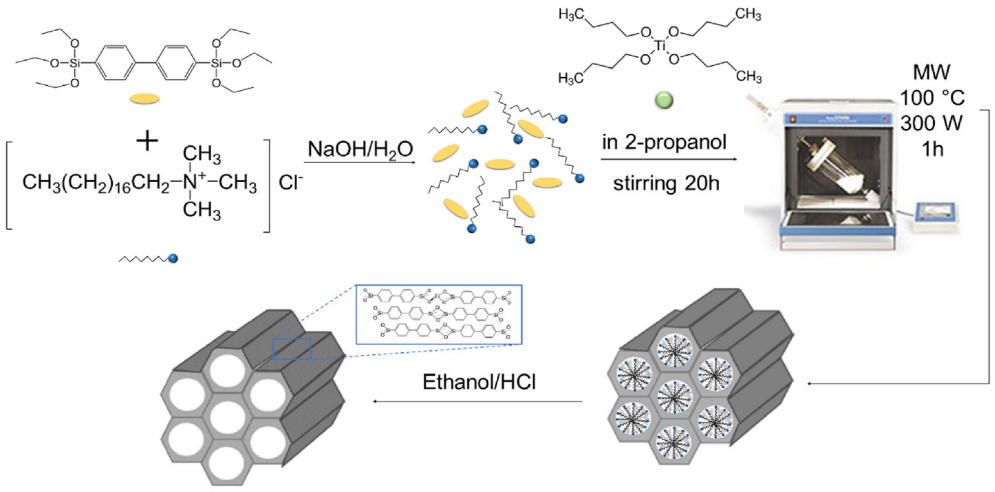

Scheme 1 – Synthetic route of Ti-PMOs.

Table 1 – Titanium content, textural properties and band gap values of Ti-PMOs and PMO.

Sample	Ti (wt%)	Si/Ti (mol/mol)	BET ($m^2\ g^{-1}$)	pore volume ($cm^3\ g^{-1}$)	pore diameter (nm)	Band gap (eV)
Ti10-PMO	1.65	10.83	829	0.84	4.2	3.65
Ti20-PMO	0.82	22.84	806	0.63	3.6	3.83
Ti40-PMO	0.52	35.48	742	0.52	3.1	3.91
PMO	–	–	871	0.69	2.9	3.95

2.2. *Photocatalytic tests*

The tests were carried out at atmospheric pressure and 293 K in a water-cooled jacketed glass reactor of 300 mL capacity under continuous gas flow operation. The reactor is equipped with a medium pressure vapor UV–visible mercury arc lamp (Ace-Hanovia), placed inside the reactor in a water-cooled quartz tube submerged in the substrate solution, and a condenser at the outlet, kept at 258 K. Before the photocatalytic reaction, the photocatalysts were degassed under vacuum at 373 K for 12 h, and then transferred to the photoreactor. In all cases, 370 mg of photocatalyst and 250 mL of an ethanol$_{(aq)}$ (25% v/v) solution previously purged with Ar, were used. After 30 min of stirring under Ar flow and dark conditions, the suspension was irradiated and after 10 min of light-on, the outlet flow was periodically measured and sampled. The evolved gaseous products were on-line analyzed by gas chromatography using a gas micro-chromatograph Varian CP-4900 with two channels and TCD detectors (detection limit for H_2, 50 ppm); the channels are equipped with M5A (10 m) and PPQ (10 m) columns that use Ar and He as carrier, respectively.

The corresponding experiments under dark, and the blank test without photocatalyst were carried out; no products were detected in gas phase in any case.

The apparent quantum efficiency (AQE) is calculated with respect the number of electrons used in the hydrogen generation [28]:

$$\text{AQE}\ (\%) = \left(\frac{\text{number of evolved } H_2 \text{ molecules x 2}}{\text{number of incident photons}}\right) \text{x } 100$$

The estimated number of incident photons capable to generate a couple e^-/h^+ was calculated from the measured radiated watt density at the exterior wall of the quartz tube (31.7 mW cm^{-2}) and the spectral lines having higher energy than 3.65 eV for Ti-PMOs (2.76×10^{18} photons s^{-1}) and 3.1 eV for TiO_2 (P25) (4.52×10^{18} photons s^{-1}).

At the end of the reaction test (4 h), the filtered liquid products were separately analyzed by gas chromatography using a Bruker 450 GC equipped with CP-Sil 8 CB 30 m × 0.25 mm CP5860 and WAX columns and a FID detector.

3. Results and discussion

3.1. *Characteristics and properties of Ti-PMOs*

Table 1 shows the Ti content and several textural characteristics of the new biphenylene-bridged Ti-PMOs, and PMO materials. All Ti-PMOs were mesoporous materials with high surface area (742–829 m^2g^{-1}), the corresponding adsorption/desorption N_2 isotherms are depicted in the Fig. S1; Ti-PMOs show surface areas slightly lower and pore diameter slightly higher than the sample without Ti, PMO (871 m^2g^{-1}, 2.9 nm pore size). For Ti-PMOs, the higher Si/Ti ratio, the lower surface area and pore diameter values.

Figs. 1 and 2 show the XRD patterns of samples in the low-angle zone ($0.2<2\theta<5^\circ$) and in the medium scattering angles ($2\theta = 4–50^\circ$), respectively. XRD patterns of PMO correspond well with that expected for biphenylene-bridged silsesquioxane with a mesoscopically ordered structure and molecular-scale periodicity in the pore-walls [27]. XRD patterns of Ti-PMO samples point out that Ti-PMOs mostly keep the structural characteristics of PMO with the incorporation of Ti in the PMO framework. The presence of a peak at about 2θ of 2° indicates the presence of mesoscopically ordered structures [27]; however, the corresponding *d* spacing increased with the Ti content (d = 41.8 Å, 44.6 Å and 49.9 Å for Ti40-PMO, Ti20-PMO and Ti10-PMO, respectively), this could be indicative of the introduction of Ti in the framework of PMO. For Ti10-PMO, with the highest content of Ti, the intensity and the shape of the peak (Fig. 1) indicate a partial loss of the ordered structure. Besides the peak at about 2θ of 2°, XRD patterns of PMO and Ti-PMOs show five well-defined peaks at medium scattering angles ($2\theta = 4–50^\circ$) (Fig. 2). The corresponding *d* spacing values, which are similar for PMO and Ti-PMO samples are 11.5 Å, 5.9 Å, 3.9 Å, 2.9 Å and 2.5 Å. A periodicity with a spacing of 11.5 Å and higher-order reflections could account for the patterns in Fig. 2 [27]. We propose that both the ordered mesoporous structure and the crystal-like molecular-scale periodicity of the pore walls [27], are kept in a major extension at least in the new Ti40-PMO and Ti20-PMO samples.

Ti20-PMO was analyzed by TEM-HRTEM. Fig. 3a clearly shows the presence of uniform mesoporous channels

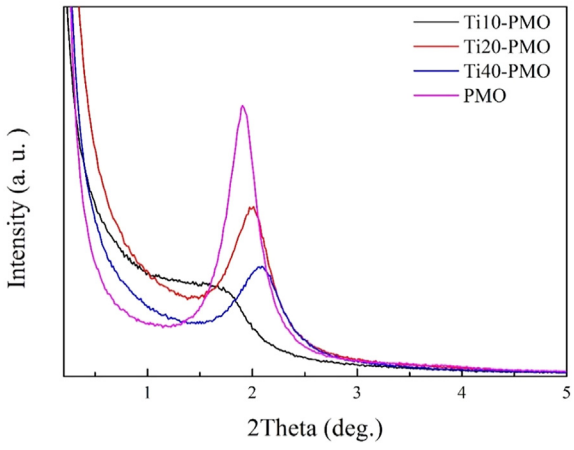

Fig. 1 – XRD patterns of Ti-PMOs and PMO in the low-angle region ($0.2^\circ<2\theta<5^\circ$).

regularly distributed. In Fig. 3b, uniform and parallel channels with wavy contrast of 4.5 nm can be seen. The electron diffraction pattern in the inset of Fig. 3b shows spots at 45 Å corresponding to the size of the parallel channels; the diffraction ring at 10.8 Å is consistent with the molecular periodicity of biphenylene groups determined by XRD.

Raman and infrared spectra of Ti-PMOs were very similar to those of PMO, Figs. S2 and S3, respectively. Raman bands of the bridged-biphenyl groups can be identified in Ti-PMOs and PMO spectra (Fig. S2). The spectra are dominated by the υ(ring-CC) band at 1599 cm^{-1}, other bands at 1512 cm^{-1} and 1135 cm^{-1} assigned to $\delta(C-H)_{i.p.}$ and at 1282 cm^{-1}, assigned to central υ(C–C), are also clearly visible in all cases [29].

Infrared spectra of PMO and Ti-PMOs samples are more complex (Fig. S3). Besides the main wide band assigned to Si–O–Si (1110-990 cm^{-1}) the presence of other clear and well defined bands characteristic of biphenyl groups can be observed: 3073 and 3027 cm^{-1} (υ(C–H)), 1602 and 1003 cm^{-1} (υ(ring-CC)), 1385 cm^{-1} (σ(ring-CH)), 1200 cm^{-1} (inter ring stretching vibration), and 807 and 703 cm^{-1} bending CC and CH, respectively [29–31].

The diffuse reflectance UV–vis spectra of PMO and Ti-PMOs are also very similar (Fig. 4). Although the broad band centred at 250–300 nm is related with the presence of biphenylene groups [32–34], for Ti-PMOs, one can expect that isolated tetrahedral Ti^{4+} species in the Ti-PMOs structure could also contribute to it [20,35]. The Ti10-PMO photocatalyst that contains the highest Ti content shows a shoulder in the band, which extends above 300 nm, this shoulder could be related with the presence of octahedral Ti^{4+} species [36].

The UV–vis DRS analysis can be used to obtain the band-gap values. The Kubelka–Munk formalism was used to convert the reflectance into the equivalent absorption coefficient, $F(R_\infty)$, and the band-gap values (Table 1) were calculated using the Tauc plot, $(F(R_\infty)\cdot h\upsilon)^n$ ($n = 0.5$) versus hυ, following the approach reported in [37] (Fig. S4). Note that the band-gap values of the photocatalysts were above those of pure TiO_2 anatase, rutile, or P25, 3.2 eV, 3.0 eV and 3.1 eV, respectively [38–40], and the band gap of Ti-PMOs, slightly decreases with the Ti content.

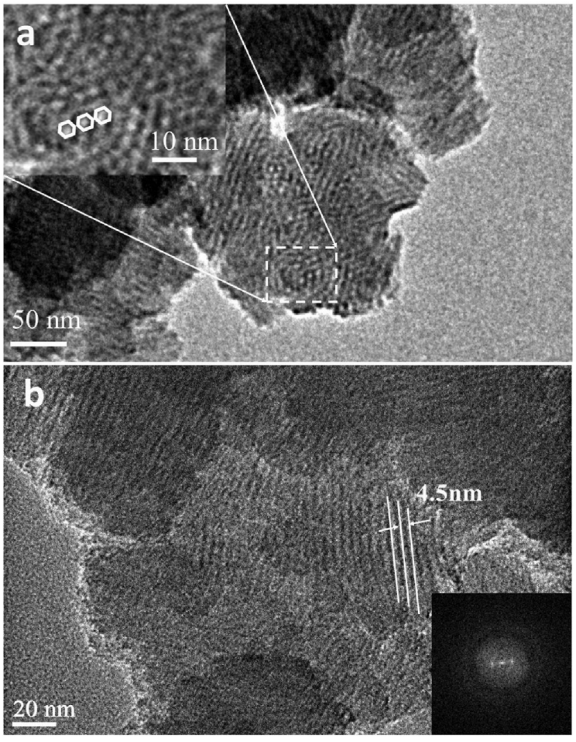

Fig. 3 – TEM images of the Ti20-PMO sample: a) in the inset, [001] incidental beam parallel to the channels in the marked zone (inset); b) in the marked zone, [100] incidental beam perpendicular to the channels. In the inset, electron diffraction pattern with spots at 4.5 nm and ring diffraction at 1.08 nm.

Ti-PMOs materials were characterized by XPS; for Ti10-PMO and Ti20-PMO, two peaks corresponding to Ti $2p_{3/2}$ and Ti $2p_{1/2}$ levels can be clearly observed (Fig. 5); the intensity of the Ti 2p spectrum corresponding to the sample Ti40-PMO is very low and does not allow an appropriate analysis of the Ti species on the surface. The Ti $2p_{3/2}$ peak of Ti20-PMO, centred at 459.7 eV, can be related with the presence of tetrahedral Ti(IV) [41–43], according to the intercalation of Ti(IV) in the

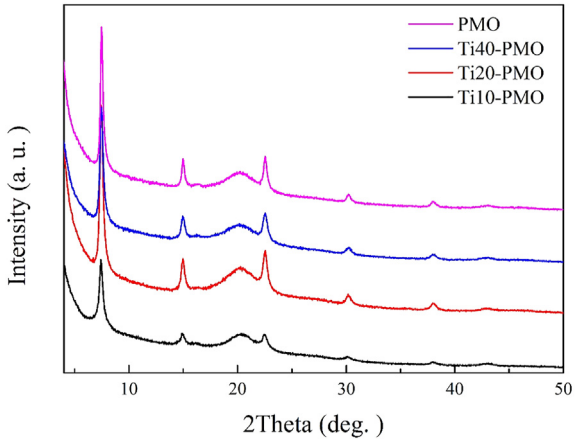

Fig. 2 – XRD patterns of Ti-PMOs and PMO in the 2θ = 4–50° zone.

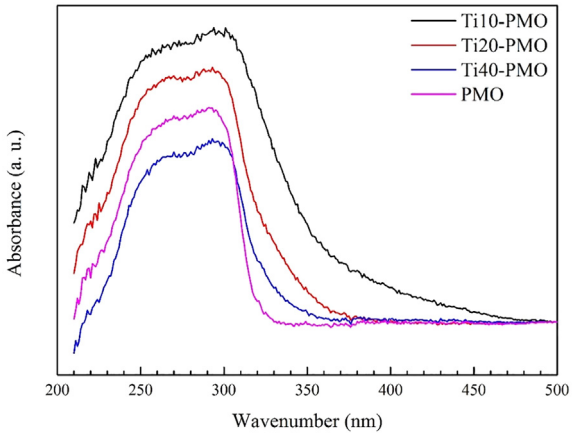

Fig. 4 – UV–visible diffuse reflectance spectra of Ti-PMOs and PMO.

PMO framework. The spectra of Ti10-PMO with the highest Ti content can be deconvoluted into two components. The component at the highest BE is related with the presence of tetrahedral Ti(IV); the component at about 458 eV could indicate the presence of octahedral Ti(IV) in Ti10-PMO [41–43], in agreement with the UV–vis DRS results.

The photoluminescence emission spectra of Ti-PMOs and PMO are shown in Fig. 6. For PMO, a broad emission peak with maximum at about 440 nm is observed, whereas for Ti-PMOs, a peak with maxima at 360–370 nm with a shoulder at higher wavelengths was obtained. The excimer emission of biphenylene groups could account for the observed bands, suggesting interactions between close biphenylene groups [22,23,44]. One could propose that in Ti-POM materials, the presence of Ti^{4+} into the framework of the POM modifies in some extension the interaction within vicinal biphenylene bridge groups.

The PL analysis of our materials (Fig. 6) shows that the intensity of the band depends on the Ti(IV) content of the samples, following the order PMO > Ti40-PMO >> Ti10-PMO > Ti20-PMO. The PL band intensity is usually related to the recombination rate of photo-induced charge carriers [45]. In general, the weaker the PL band intensity, the lower the recombination rate of the photo-induced charges; that is, the generated photoelectron has longer lifetime.

Fig. 7 shows the transient photocurrent responses spectra of Ti-PMOs and PMO samples under a simulated solar light irradiation with a pulse light on-off process; the larger photocurrent value represents the higher photoelectron yield. Ti-PMOs samples show much larger photocurrent density than PMO, with the order: Ti20-PMO > Ti10-PMO > Ti40-PMO >> PMO. The photocurrent density significantly increases with the introduction of small amounts of Ti into the PMO framework and shows a maximum for Ti20-PMO (0.82 Ti wt%) (Fig. 7).

Fig. 8 shows the EIS Nyquist plots of Ti-PMOs and PMO, which were obtained in dark (Fig. 8A) and under simulated

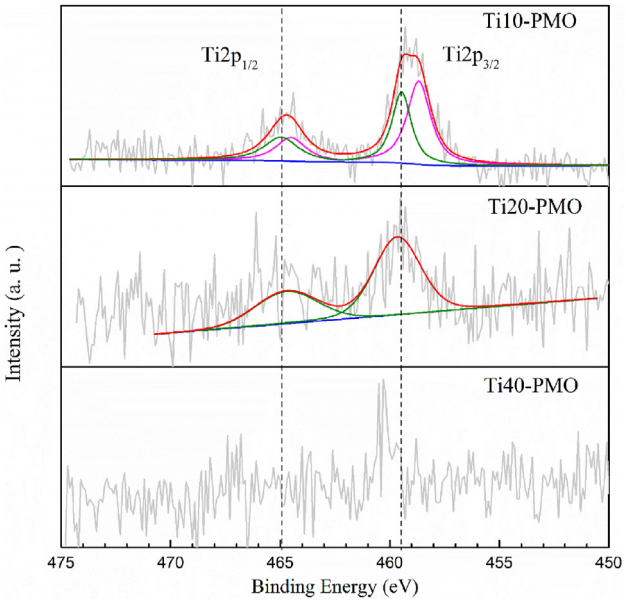

Fig. 5 – Ti 2p XP spectra of Ti-PMOs.

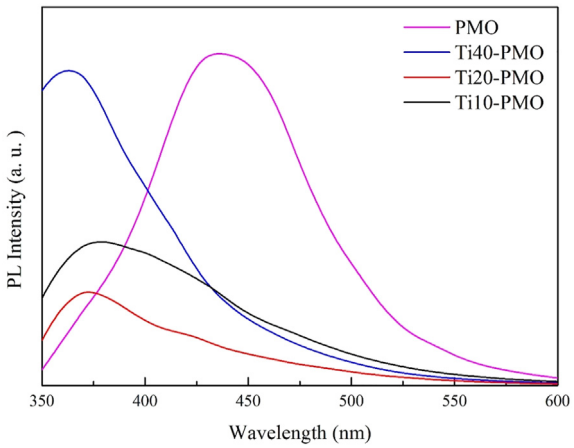

Fig. 6 – PL emission spectra of Ti-PMOs and PMO.

solar light irradiation (Fig. 8B). In all cases, the arc radius under illumination (Fig. 8B) is smaller than in dark conditions (Fig. 8A), this indicates a decrease of the barrier for the transfer of photogenerated electrons under irradiation. Moreover, in both cases, under illumination and in dark conditions, Ti-PMOs samples show smaller arc radius than PMO. This clearly indicates that the presence of Ti species in the framework of PMO reduces the transport resistance of the photogenerated electrons. In both conditions, the Nyquist arc radius follows the order: PMO >> Ti40-PMO > Ti10-PMO > Ti20-PMO. This order corresponds well with that of photocurrent values and PL results. These results indicate that the introduction of a low amount of Ti into the framework of PMO produces an increase of the photoelectron yield and of the charge separation efficiency. Besides, a decrease of the barrier for the electron transfer is noted.

For Ti-PMOs photocatalysts, upon light absorption, a LMCT process could occur with a long-lived excited charge separation state, transferring the electron from the organic entity to the Ti^{4+} center [46]. The radiative decay process from the excited state to the ground state could be slow down when highly dispersed Ti species having a tetrahedral coordination are introduced into the PMO framework. These effects were more significant for the sample Ti20-PMO, which showed by XPS the presence of only tetrahedral Ti^{4+} species into the PMO framework and kept the ordered mesoporous structure and the crystal-like molecular-scale periodicity of the pore walls; although Ti40-PMO and Ti20-PMO have similar structural characteristics, the amount of Ti^{4+} in the later is higher. On the other hand, in Ti10-PMO, which had a higher titanium content, a partial loss of the ordered structure took place and the presence of octahedral Ti^{4+} likely PMO extra-framework species was determined.

3.2. *Photocatalytic behavior*

The photocatalytic production of H_2 from aqueous solutions of ethanol was determined as indicated in the Materials and methods section.

Fig. 9 shows the total amount of H_2 produced during the 4 h of photocatalytic test. As can be observed, the Ti-PMOs presented higher activity than that of PMO; the amount of H_2

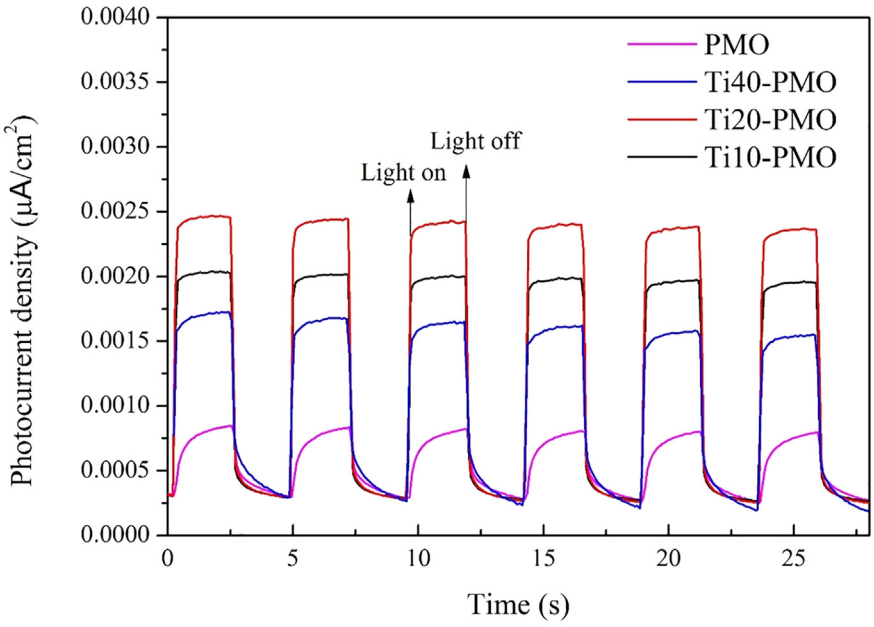

Fig. 7 – Photocurrent response of Ti-PMOs and PMO.

produced followed the order: Ti20-PMO > Ti10-PMO > Ti40-PMO > PMO, which is in very good agreement with the photoelectrochemical results discussed above. The TiO_2 reference (P25) photocatalyst was much less active than the hybrid materials (Fig. 9). The sequence was kept when the H_2 yield per m^2 is considered (Fig. S5). The Ti centre in the hybrid Ti-PMOs material can facilitate the photogenerated charge separation and electron transfer for H^+ reduction, meanwhile the holes oxidize the alcohol. Among the Ti-PMOs, Ti20-PMO, produced the highest amount of H_2 (Fig. 9). The photocatalytic behavior of Ti20-PMO can be related with its photoelectrochemical characteristics; Ti20-PMO showed the lowest intensity of PL band (Fig. 6) and the lowest transport resistance (Fig. 8), which are related with a lower velocity of charge recombination, thus resulting in the highest transient photocurrent response (Fig. 7). As stated above, we relate these characteristics of Ti20-PMO with the presence of well dispersed tetrahedral Ti^{4+} centers into the PMO framework. A high dispersion of tetrahedral Ti^{4+} in other Ti-containing mesoporous materials such as Ti-MCM-48 and Ti-MCM-41 has been previously related with a high photocatalytic activity in H_2 production [47,48].

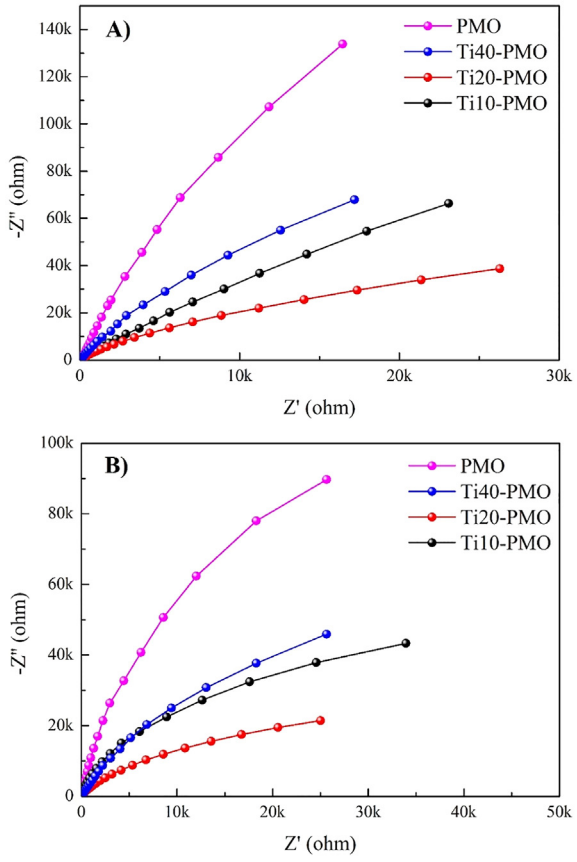

Fig. 8 – EIS Nyquist plots of Ti-PMOs and PMO: A) in dark; B) under irradiation.

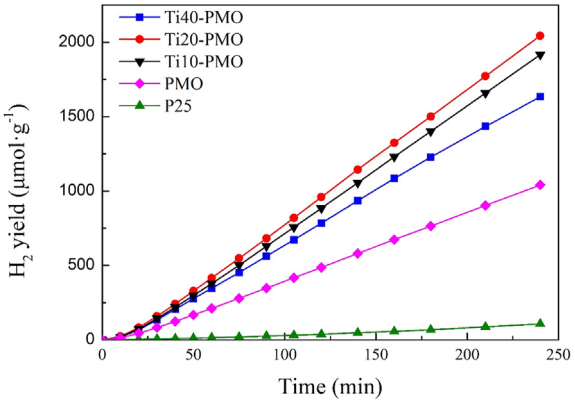

Fig. 9 – Total amount of H_2 produced from ethanol$_{(aq)}$ 25% v/v with Ti-PMOs, PMO and P25 photocatalysts during 4 h of test; T = 293 K.

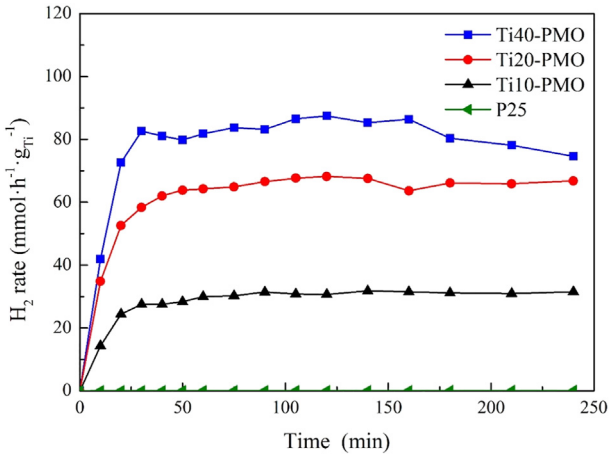

Fig. 10 – H_2 production rate (mmol/h.g_{Ti}) from ethanol$_{(aq)}$ 25% v/v with Ti-PMOs and reference TiO_2(P25) photocatalysts during 4 h under UV–vis irradiation; T = 293 K.

The calculated AQE values are shown in Fig. S6. AQE values are very useful to compare the performance of different catalysts for the same reaction. Nevertheless, AQE depends on the experimental conditions of the photocatalytic test, including for a given catalyst the excitation wavelength; this hinders a straightforward comparison of different data in the bibliography [49]. However, within the photocatalysts studied in this work, it is shown that Ti-PMOs are much more efficient photocatalytic systems than TiO_2 (P25); moreover, the introduction of Ti in the PMO framework enhances the photocatalytic activity. The highest AQE was 0.36% for Ti20-PMO photocatalyst, which is remarkably higher than that obtained for TiO_2 (P25) (0.02%) under the experimental conditions used. In order to rationalize the photoactivity of Ti-PMOs, Fig. 10 shows the rate of H_2 production referred to the Ti content during the 4 h of photocatalytic test. As can be observed Ti-PMOs are much more effective than reference TiO_2. Among Ti-PMOs, Ti10-PMO exhibited the lowest H_2 production rate per Ti centre. For this sample, with the highest Ti content among the Ti-PMOs materials, besides tetrahedral Ti(IV), the presence of octahedral TI(IV) species was found.

Finally, it can be observed a rather stable H_2 production rate for Ti-PMO photocatalysts during the photocatalytic test; no apparent deactivation occurs along the reaction time analyzed (Fig. 10). In order to verify this aspect, Ti-PMOs were characterized by several techniques after the photocatalytic transformation of ethanol aqueous solution. XRD patterns of fresh and used catalysts were similar (Fig. S7), indicating that both the ordered mesoporous structure and the crystal-like molecular-scale periodicity of the pore walls resulted unmodified after the photocatalytic test. Moreover, no relevant variation of the adsorption/desorption N_2 isotherms (Fig. S8) and BET surface area (Table S2) took place. The infrared spectra of fresh and used catalysts were also similar (Fig. S9). These results point to a good stability of the Ti-PMO materials under the conditions of photocatalytic test.

In the photocatalytic study carried out in this work, besides H_2, 2,3-butanediol and minor amounts of CO, CH_4, C_2H_4 and CH_3CHO were obtained (Table S1); O_2 or CO_2 were not detected. The formation of 2,3-butanediol using ethanol as a sacrificial reagent has been proposed via the coupling of two α-hydroxyethyl radicals (·$CH(OH)CH_3$) [50] (Eq. (1)), (Fig. 11).

$$2\cdot CH(OH)CH_3 \rightarrow CH_3CH(OH)CH(OH)CH_3 \quad (1)$$

The formation of α-hydroxyethyl radicals (Eq. (2)) has been proposed to be the first step for the formation of acetaldehyde (Eq. (3)) and 2,3-butanediol (Eq. (1)) [24–26,50].

$$CH_3CH_2OH + h^+ \rightarrow \cdot CH(OH)CH_3 + H^+ \quad (2)$$

$$\cdot CH(OH)CH_3 + h^+ \rightarrow CH_3CHO + H^+ \quad (3)$$

$$2H^+ + 2e^- \rightarrow H_2 \quad (4)$$

We relate the 2,3-butanediol formation with the pore characteristics of Ti-PMOs photocatalysts as it has been shown for other TiO_2-based systems; a higher amount of 2,3-butanediol has been found when Pt/TiO_2 photocatalysts with a smaller pore size (in the range 4.5–30 nm) have been used [25].

The no obtention of acetic acid or CO_2, points that successive oxidation pathways of acetaldehyde are minor.

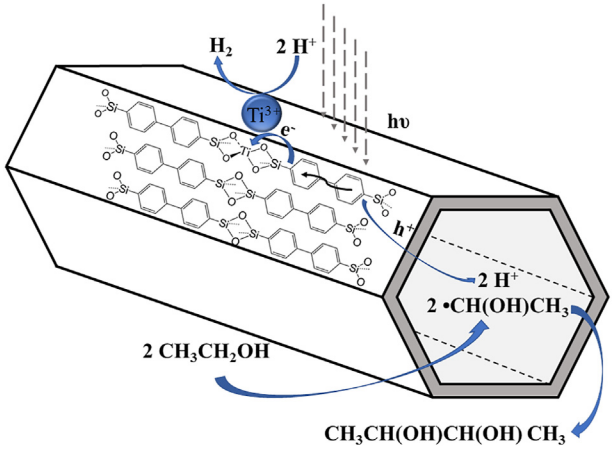

Fig. 11 – Photocatalytic ethanol transformation over Ti-PMOs photocatalysts.

4. Conclusions

New Ti-containing periodic mesoporous organosilicas with biphenylene moieties, Ti-PMOs (Si/Ti = 10–40 mol/mol), were prepared following a simple microwave-assisted method. Ti-PMOs showed high surface-areas (742–829 m^2g^{-1}), pore size about 3–4 nm, molecular-scale periodicity in the pore walls and mesoscopically ordered structures.

The Ti-PMOs hybrid materials were active in the photocatalytic transformation of aqueous ethanol (25% v/v) without assistance of noble metal co-catalyst. The main products obtained were H_2 and 2,3-butanediol. Both, the total H_2 produced and the H_2 produced per m^2, were higher when Ti-PMOs photocatalysts were used compared to PMO and reference

P25. Ti20-PMO showed the best photocatalytic behavior, it produced about 508 μmol H_2 g_{cat}^{-1} h^{-1} with an apparent quantum efficiency of 0.36%; Ti20-PMO showed a stable H_2 production rate during the photocatalytic test. The presence of tetrahedral Ti(IV) centers in Ti20-PMO framework is related with a lower velocity of (e^-/h^+) charge recombination, an easier charge transfer and a higher photocatalytic activity. After the photocatalytic test, structural and textural characteristics of Ti-PMOs were kept.

Declaration of Competing Interest

The authors declare that they have no known competing financial interests or personal relationships that could have appeared to influence the work reported in this paper.

Acknowledgements

The authors thank MAT2017-87500-P project for financial support. Y. W. thanks the China scholarship Council for his PhD grant CSC201608460014. Dr. F. Güell is acknowledged for PL measurements and, CCiT-UB and IREC for technical services.

Appendix A. Supplementary data

Supplementary data to this article can be found online at https://doi.org/10.1016/j.jmrt.2021.07.104.

REFERENCES

[1] Cargnello M, Gasparotto A, Gombac V, Montini T, Barreca D, Fornasiero P. Photocatalytic H_2 and added-value by products - the role of metal oxide systems in their synthesis from oxygenates. Eur J Inorg Chem 2011:4309–23. https://doi.org/10.1002/ejic.201100532.

[2] Bowker M. Sustainable hydrogen production by the application of ambient temperature photocatalysis. Green Chem 2011;13:2235–46. https://doi.org/10.1039/C1GC00022E.

[3] Dal Santo V, Gallo A, Naldoni A, Guidotti M, Psaro R. Bimetallic heterogeneous catalysts for hydrogen production. Catal Today 2012;197:190–205. https://doi.org/10.1016/j.cattod.2012.07.037.

[4] Navarro RM, Arenales J, Vaquero F, González ID, Fierro JLG. The effect of Pt characteristics on the photoactivity of Pt/TiO_2 for hydrogen production from ethanol. Catal Today 2013;210:33–8. https://doi.org/10.1016/j.cattod.2013.01.006.

[5] López CR, Melián EP, Ortega Méndez JA, Santiago DE, Doña Rodríguez JM, González Díaz O. Comparative study of alcohols as sacrificial agents in H_2 production by heterogeneous photocatalysis using Pt/TiO_2 catalysts. J Photochem Photobiol A Chem 2015;312:45–54. https://doi.org/10.1016/j.jphotochem.2015.07.005.

[6] Chiarello GL, Dozzi MV, Selli E. TiO_2-based materials for photocatalytic hydrogen production. J Energy Chem 2017;26:250–8. https://doi.org/10.1016/j.jechem.2017.02.005.

[7] Ibrahim NS, Leaw WL, Mohamad D, Aliasc SH, Nur H. A critical review of metal-doped TiO_2 and its structure–physical properties–photocatalytic activity relationship in hydrogen production. Int J Hydrogen Energy 2020;45:28553–65. https://doi.org/10.1016/j.ijhydene.2020.07.233.

[8] Matsuoka M, Anpo M. Local Structures, Excited States, and Photocatalytic reactivities of highly dispersed catalysts constructed within zeolites. J Photochem Photobiol C: Photochem Rev 2003;3:225–52. https://doi.org/10.1016/S1389-5567(02)00040–0.

[9] Do YJ, Kim JH, Park JH, Park SS, Hong SS, Suh CS, et al. Photocatalytic decomposition of 4-nitrophenol on Ti-containing MCM-41. Catal Today 2005;101:299–305. https://doi.org/10.1016/j.cattod.2005.03.009.

[10] Shiraishi Y, Morishita M, Hirai T. Acetonitrile-assisted highly selective photocatalytic epoxidation of olefins on Ti-containing silica with molecular oxygen. Chem Commun 2005;48:5977–9. https://doi.org/10.1039/B512807B.

[11] Zeng L, Guo X, He C, Duan C. Metal–organic frameworks: versatile materials for heterogeneous photocatalysis. ACS Catal 2016;6:7935–47. https://doi.org/10.1021/acscatal.6b02228.

[12] Valverde-González A, López Calixto CG, Barawi M, Gomez-Mendoza M, de la Peña O'Shea VA, Liras M, et al. Understanding charge transfer mechanism on effective truxene-based porous polymers–TiO_2 hybrid photocatalysts for hydrogen evolution. ACS Appl Energy Mater 2020;3:4411–20. https://doi.org/10.1021/acsaem.0c00118.

[13] Zhu J, Li PZ, Guo W, Zhao Y, Zou R. Titanium-based metal–organic frameworks for photocatalytic applications. Coord Chem Rev 2018;359:80–101. https://doi.org/10.1016/j.ccr.2017.12.013.

[14] Wang CC, Wang X, Liu W. The synthesis strategies and photocatalytic performances of TiO_2/MOFs composites: a state-of-the-art review. Chem Eng J 2020;391:123601. https://doi.org/10.1016/j.cej.2019.123601.

[15] López-Calixto CG, Barawi M, Gomez-Mendoza M, Oropeza F, Fresno F, Liras M, et al. Hybrids Based on BOPHY-conjugated porous polymers as photocatalysts for hydrogen production: insight into the charge transfer pathway. ACS Catal 2020;10:9804–12. https://doi.org/10.1021/acscatal.0c01346.

[16] Asefa T, MacLachlan MJ, Coombs N, Ozin GA. Periodic mesoporous organosilicas with organic groups inside the channel walls. Nature 1999;402:867. https://doi.org/10.1038/47229.

[17] Inagaki S, Guan S, Fukushima Y, Ohsuna T, Terasaki O. Novel mesoporous materials with a uniform distribution of organic groups and inorganic oxide in their frameworks. J Am Chem Soc 1999;121:9611–4. https://doi.org/10.1021/ja9916658.

[18] Inagaki S, Guan S, nOhsuna T, Terasaki O. An ordered mesoporous organosilica hybrid material with a crystal-like wall structure. Nature 2002;416:304. https://doi.org/10.1038/416304a.

[19] Polarz S, Kuschel A. Preparation of a periodically ordered mesoporous organosilica material using chiral building blocks. Adv Mater 2006;18:1206–9. https://doi.org/10.1002/adma.200502647.

[20] Morishita M, Shiraishi Y, Hirai T. Ti-containing mesoporous organosilica as a photocatalyst for selective olefin epoxidation. J Phys Chem B 2006;110:17898–905. https://doi.org/10.1021/jp062355w.

[21] Mizoshita N, Ikai M, Tani T, Inagaki S. Hole-transporting periodic mesostructured organosilica. J Am Chem Soc 2009;131:14225–7. https://doi.org/10.1021/ja9050263.

[22] Yamanaka KI, Okada T, Goto Y, Tani T, Inagaki S. Dynamics in the excited electronic state of periodic mesoporous biphenylylene-silica studied by time-resolved diffuse reflectance and fluorescence spectroscopy. Phys Chem Chem Phys 2010;12:11688–96. https://doi.org/10.1039/C004255B.

[23] Okada T, Yamanaka KI, Hirose Y, Goto Y, Tani T, Inagaki S. Fluorescence studies on phenylene moieties embedded in a framework of periodic mesoporous organosilica. Phys Chem Chem Phys 2011;13:7961–7. https://doi.org/10.1039/C0CP02714F.

[24] Sola AC, Homs N, Ramírez de la Piscina P. Photocatalytic H_2 production from ethanol$_{(aq)}$ solutions: the effect of intermediate products. Int J Hydrogen Energy 2016;41:19629–36. https://doi.org/10.1016/j.ijhydene.2016.05.268.

[25] Sola AC, Ramírez de la Piscina P, Homs N. Behaviour of Pt/TiO_2 catalysts with different morphological and structural characteristics in the photocatalytic conversion of ethanol aqueous solutions. Catal Today 2020;341:13–20. https://doi.org/10.1016/j.cattod.2018.06.017.

[26] Pajares A, Wang Y, Kronenberg MJ, Ramírez de la Piscina P, Homs N. Photocatalytic H_2 production from ethanol aqueous solution using TiO_2 with tungsten carbide nanoparticles as co-catalyst. Int J Hydrogen Energy 2020;45:20558–67. https://doi.org/10.1016/j.ijhydene.2020.04.010.

[27] Kapoor MP, Yang Q, Inagaki S. Self-assembly of biphenylene-bridged hybrid mesoporous solid with molecular-scale periodicity in the pore walls. J Am Chem Soc 2002;124:15176–7. https://doi.org/10.1021/ja0290678.

[28] Braslavsky SE, Braun AM, Cassano AE, Emeline AV, Litter MI, Palmisano L, et al. Glossary of terms used in photocatalysis and radiation catalysis (IUPAC Recommendations 2011). Pure Appl Chem 2011;83:931–1014. https://doi.org/10.1351/PAC-REC-09-09-36.

[29] Hoffmann F, Güngerich M, Klar PJ, Fröba M. Vibrational spectroscopy of Periodic mesoporous organosilicas (PMOs) and their precursors: a closer look. J Phys Chem C 2007;111:5648–60. https://doi.org/10.1021/jp0668596.

[30] Constantinidis P, Schmitt HC, Fischer I, Yan B, Rijs AM. Formation of polycyclic aromatic hydrocarbons from bimolecular reactions of phenyl radicals at high temperatures. Phys Chem Chem Phys 2015;17:29064–71. https://doi.org/10.1039/C5CP05354D.

[31] Katon JE, Lippincott ER. The vibrational spectra and geometrical configuration of biphenyl. Spectrochim Acta 1959;15:627–50. https://doi.org/10.1016/S0371-1951(59)80360-X.

[32] Goto Y, Mizoshita N, Ohtani O, Okada T, Shimada T, Tani T, et al. Synthesis of mesoporous aromatic silica thin films and their optical properties. Chem Mater 2008;20:4495–8. https://doi.org/10.1021/cm800492s.

[33] Ohashi M, Aoki M, Yamanaka KI, Nakajima K, Ohsuna T, Tani T, et al. A periodic mesoporous organosilica-based donor–acceptor system for photocatalytic hydrogen evolution. Chem A Eur J 2009;15:13041–6. https://doi.org/10.1002/chem.200901721.

[34] Gao M, Han S, Qiu X, Wang H. Biphenyl-bridged periodic mesoporous organosilicas: synthesis and in situ charge-transfer properties. Microporous Mesoporous Mater 2014;198:92–100. https://doi.org/10.1016/j.micromeso.2014.07.021.

[35] Ikeue K, Yamashita H, Anpo M, Takewaki T. Photocatalytic reduction of CO_2 with H_2O on Ti–β Zeolite photocatalysts: effect of the hydrophobic and hydrophilic properties. J Phys Chem B 2001;105:8350–5. https://doi.org/10.1021/jp010885g.

[36] Huang Y, Yuan P, Wu Z, Yuan X. Preparation of surface-silylated and benzene-bridged, Ti-containing mesoporous silica for cyclohexene epoxidation. J Porous Mater 2016;23:895–903. https://doi.org/10.1007/s10934-016-0146-7.

[37] Makuła P, Pacia M, Macyk W. How to correctly determine the band gap energy of modified semiconductor photocatalysts based on UV–Vis spectra. J Phys Chem Lett 2018;9:6814–7. https://doi.org/10.1021/acs.jpclett.8b02892.

[38] Leung DYC, Fu X, Wang C, Ni M, Leung MKH, Wang X, et al. Hydrogen production over titania-based photocatalysts. ChemSusChem 2010;3:681–94. https://doi.org/10.1002/cssc.201000014.

[39] Shimura K, Yoshida H. Heterogeneous photocatalytic hydrogen production from water and biomass derivatives. Energy Environ Sci 2011;4:2467–81. https://doi.org/10.1039/C1EE01120K.

[40] Fontelles-Carceller O, Muñoz-Batista M, Rodríguez-Castellón E, Conesa J, Fernández-García M, Kubacka A. Measuring and interpreting quantum efficiency for hydrogen photo-production using Pt-titania catalysts. J Catal 2017;347:157–69. https://doi.org/10.1016/j.jcat.2017.01.012.

[41] Chu H, Wan CY, Zhao D. Synthesis of ordered mesoporous bifunctional TiO_2–SiO_2–polymer nanocomposites. J Mater Chem 2009;19:8610–8. https://doi.org/10.1039/B911107G.

[42] Barrio L, Campos-Martín JM, de Frutos-Escrig MP, Fierro JLG. Selective grafting of titanium on periodic nanoporous silica materials. Microporous Mesoporous Mater 2008;113:542–53. https://doi.org/10.1016/j.micromeso.2007.12.014.

[43] Chandra D, Mal NK, Mukherjee M, Bhaumik A. Titanium-rich highly ordered mesoporous silica synthesized by using a mixed surfactant system. J Solid State Chem 2006;179:1802–7. https://doi.org/10.1016/j.jssc.2006.03.020.

[44] Cione AP, Scaiano JC, Neumann MG, Gessner F. The excimer emission of aromatic hydrocarbons on clays. J Photochem Photobiol A 1998;118:205–9. https://doi.org/10.1016/S1010-6030(98)00379–7.

[45] Liqiang J, Yichun Q, Baiqi W, Shudan L, Baojiang J, Libin Y, et al. Review of photoluminescence performance of nano-sized semiconductor materials and its relationships with photocatalytic activity. Sol Energy Mater Sol Cells 2006;90:1773–87. https://doi.org/10.1016/j.solmat.2005.11.007.

[46] Fu Y, Sun D, Chen Y, Huang R, Ding Z, Fu X, et al. An Amine-functionalized titanium metal–organic framework photocatalyst with visible-light-induced activity for CO_2 reduction. Angew Chem Int Ed 2012;51:3364–7. https://doi.org/10.1002/anie.201108357.

[47] Zhao D, Budhi S, Rodriguez A, Koodali RT. Rapid and facile synthesis of Ti-MCM-48 mesoporous material and the photocatalytic performance for hydrogen evolution. Int J Hydrogen Energy 2010;35:5276–83. https://doi.org/10.1016/j.ijhydene.2010.03.087.

[48] Peng R, Zhao D, Dimitrijevic NM, Rajh T, Koodali RT. Room temperature synthesis of Ti-MCM-48 and Ti-MCM-41 mesoporous materials and their performance on photocatalytic splitting of water. J Phys Chem C 2012;116:1605–13. https://doi.org/10.1021/jp210448v.

[49] Languer MP, Scheffer FR, Feil AF, Baptista DL, Migowski P, Machado GJ, et al. Photo-induced reforming of alcohols with improved hydrogen apparent quantum yield on TiO_2 nanotubes loaded with ultra-small Pt nanoparticles. Int J Hydrogen Energy 2013;38:14440–50. https://doi.org/10.1016/j.ijhydene.2013.09.018.

[50] Lu H, Zhao J, Li L, Gong L, Zheng J, Zhang L, et al. Selective oxidation of sacrificial ethanol over TiO_2-based photocatalysts during water splitting. Energy Environ Sci 2011;4:3384–8. https://doi.org/10.1039/C1EE01476E.